PAPER

Check for updates

Triboelectric charge-separable probes for potential single-droplet biochemical sensing†

Along Gao,‡[a] Boyou Wang,‡[a] Chengpai Peng,[a] Xiali Yang,[a] Man Zhang,[a] Hanyue Liu,[a] Jing Pan,[a] Hai Zhu, [ID] *[b] Qitao Zhou*[a] and Fan Xia [ID] [a]

Biochemical sensors have found widespread applications in the fields of health and environment. As the number of biochemical sensors continues to increase, their energy supply has emerged as a challenge. Self-powered biochemical sensors based on triboelectric generators (TENGs) offer a promising solution to this challenge. However, current self-powered sensors for *in situ* detection of liquid samples either suffer from low output signals, resulting in insufficient sensitivity, or require relatively large sample volumes. To address these challenges, this work introduces a TENG with charge separation capability by incorporating electrodes that can directly contact the solution at both ends of a fluidic channel. Unlike traditional devices, this device utilizes the reciprocating motion of a single droplet within the device to achieve charge accumulation in both the electrodes and the liquid sample. By utilizing the characteristic that biochemical substances contained within the droplet affect its charge storage capacity, the concentration of these biochemical substances in the droplet is reflected by the value of the output voltage when it reaches a stable state. The device functions as a triboelectric charge-separable probe and demonstrates responsiveness to solution pH, salt concentration, and the concentration of nanoparticles or *Escherichia coli*, showcasing its potential as a biochemical sensor.

Introduction

With advancements in nanoscience and nanotechnology, chemical sensing plays an indispensable role in biological diagnosis,[1,2] chemical reactions[3–5] and detection of trace toxic substances.[6,7] However, as the number of these sensors continues to grow, the issue of powering such a vast array of sensors has become a significant challenge. This is primarily due to the issues associated with charging, discharging, and replacement when solely relying on battery power, as well as the environmental problems posed by battery disposal. Therefore, harnessing renewable energy from the environment to power sensors and achieve self-sufficiency is a highly promising solution.[8–10] In recent years, triboelectric nanogenerators (TENGs) have garnered considerable attention due to their ability to harvest mechanical energy from the environment

and convert it into electrical energy, thereby enabling the construction of self-powered sensor systems.[9–15] Simultaneously, TENGs can utilize the influence of the detection target on the electron gain and loss capability of the triboelectric material surface during their operation to modulate the intensity of the output electrical signal, thereby enabling active, self-powered biochemical sensing.[16,17]

However, when detecting liquid samples, it is often difficult to ensure the strength of the signal. This is primarily due to the screening effect of salt ions in the solution, which weakens the transfer of electrons and reduces the amount of charge that can be carried on the surface of the triboelectric material. Additionally, salt ions can also neutralize a portion of the charge on the surface of the tribological material through electrostatic neutralization.[18]

In recent years, people have achieved amplification of the output electrical signal by improving the electrode structure of solid–liquid interface TENGs. Wang *et al.* developed a novel droplet-based electricity generator, featuring a transistor-inspired architecture.[19,20] Song *et al.* reported a water droplet-based high-voltage direct current TENG. The water droplet acts as a charge shuttle, which can deliver positive charges to the top electrode and negative charges to the bottom electrode.[21,22]

However, these devices achieve high output signals by continuously allowing fresh droplets to pass over their surfaces.

[a]State Key Laboratory of Geomicrobiology and Environmental Changes, Engineering Research Center of Nano-Geomaterials of Ministry of Education, Faculty of Materials Science and Chemistry, China University of Geosciences, Wuhan 430074, China. E-mail: zhouqitao@cug.edu.cn

[b]Department of Civil Engineering, The University of Hong Kong, Pokfulam 999077, Hong Kong Special Administrative Region of China. E-mail: zhuhai@hku.hk

‡These authors contributed equally to this work.

Consequently, biochemical detection through this type of device requires a relatively large sample volume.[23] Therefore, drawing inspiration from the electrode configurations of existing devices to construct self-powered sensor devices capable of detecting trace droplets holds significant importance.

In this work, a solid–liquid interface TENG is obtained by arranging two copper electrodes inside a semi-open polydimethylsiloxane (PDMS) fluidic channel. The device detects substances contained in droplets by continuously shaking the analytical solution within the solution chamber. During this shaking process, the two copper electrodes continuously facilitate charge separation, while the droplet itself simultaneously accumulates charges. By leveraging the output voltage achieved when both processes reach equilibrium, the device is able to detect the substances present in the droplets. The output performance of the device exhibits a variation in accordance with changes in the concentration of silica nanoparticles present in the liquid. As a demonstration, the device was further utilized to detect the concentration of *Escherichia coli* (*E. coli*) in tap water.

Results and discussion

The developed liquid–solid triboelectric probe system is schematically shown in Fig. 1a. The triboelectric probe is composed of a glass slide, a fluid channel, and two electrodes including top and bottom electrodes, and then a copper electrode with a needle tip is installed at the center of the bottom copper electrode. The needle functions as a charge collector, which attracts negative charges from the droplet and acts as a conduit to facilitate the transfer of these negative charges to the bottom copper electrode. Fig. 1a also shows a photograph of the triboelectric probe system and the dimensions of the device in the top view are shown in Fig. S1.† Before the test, the water contact angle of the PDMS is measured and the results are shown in Fig. S2.† The test results show that PDMS has good hydrophobic properties with a contact angle of about 118.7°, which ensures contact electrification when water comes into contact with the PDMS surface. During the test, the device is fixed on a rotary mixer. The rotation of the device induces fluid movement back and forth. As the droplet slides back and forth, it sequentially contacts the bottom needle electrode and the top copper electrode of the triboelectric probe, achieving the separation of negative and positive charges within the droplet (Movie S1†). After the separation of positive and negative charges by the triboelectric probe, the charges will be stored in the two copper electrodes, respectively, ultimately generating a voltage output.

In the aforementioned process, the circuit closes and an output current signal is generated only when the droplet comes into contact with the charge collection needle.
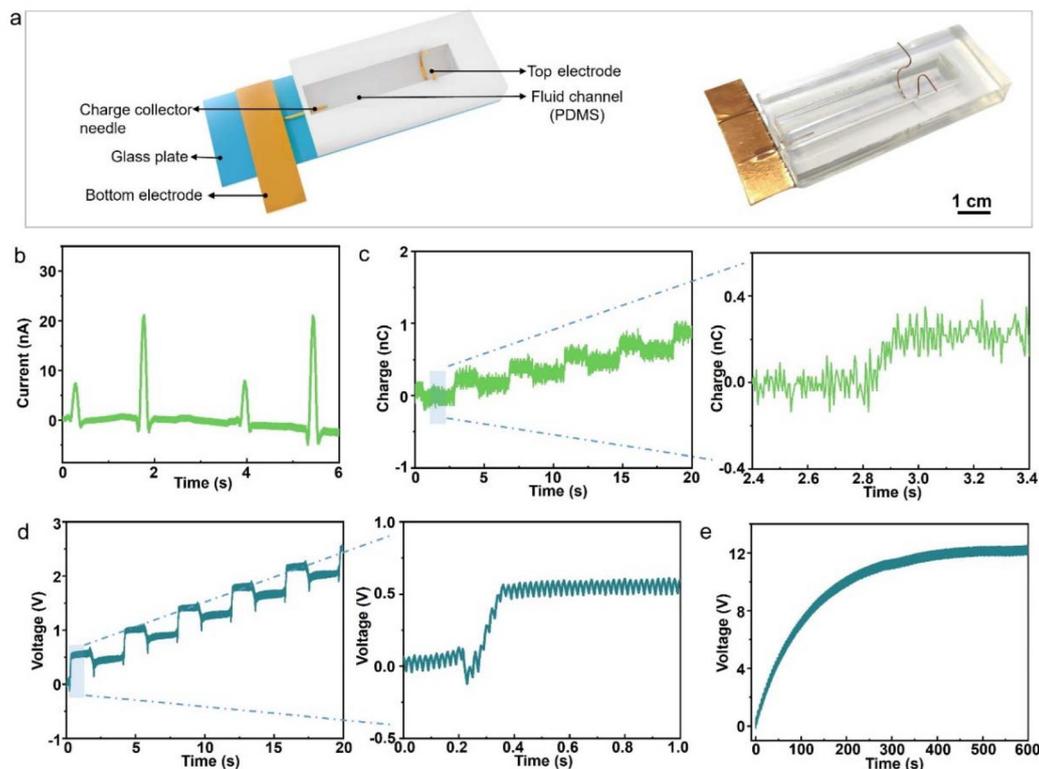

Fig. 1 The device structure and output performance of the triboelectric charge-separable probe (the type of droplet is deionized water). (a) Schematic diagram and image of the device structure. (b) Variation of device output current over time. (c) Characterization of device transferred charge. (d) and (e) Output voltage signal of the device.

Subsequently, as the droplet moves away from the needle and continues downward, it makes contact with the top electrode. At this moment, the circuit is immediately reconnected and another output current signal is obtained (Fig. 1b). Moreover, after the droplet repeatedly comes into contact with the charge collection needle and top electrode, the two electrodes of the triboelectric probe act like reservoirs, continuously storing the charge generated by the impact of the droplet under open-circuit conditions and enabling a monotonic and sustained increase in both the transferred charge and the output voltage of the device. As shown in Fig. 1c and d, approximately a charge of 0.4 nC and a voltage of 0.5 V are collected in each operational cycle. When the potential difference between the droplet and the collection needle is balanced, the voltage of the triboelectric probe reaches its maximum value of approximately 12 V (Fig. 1e). In addition, the maximum instantaneous power density output of 0.045 mW m^{-3} is achieved when the external loading resistance is set to 6 MΩ (Fig. S3†).

To elucidate the working mechanism of the triboelectric probe, Fig. 2 illustrates the charge distribution of the droplet in one operating cycle. In the "Wang" model, the electric double layer formation is a two-step process. Initially, electrons are transferred from water molecules to the solid atoms upon contact between the liquid and the solid. Subsequently, the charged solid surface attracts opposite charges from the liquid via electrostatic interactions, resulting in the establishment of the electric double layer. This process begins with electron transfer and ion adsorption and continues with the attraction and adsorption of free ions onto the charged solid surface, driven by electrostatic forces. Consequently, when the droplet flows over the PDMS, the strong affinity of PDMS to electrons results in the acquisition of electrons from the droplet, which in turn leads to the creation of positively charged hydrated hydrogen ions (H_3O^+). The H_3O^+ ions will adhere to the solid surface as a result of electrostatic attraction, which aids in the formation of the electric double layer.[24] The above process primarily involves generating surface charges on the triboelectric material. This process has been widely recognized, and this work primarily discusses the subsequent processes. Then, by spreading the droplet, the negatively charged PDMS is electrically screened by the positive ions, migrating and/or diffusing negative charges on the surface (Fig. 2i). Subsequently, as the device deflects, the droplet flows back and forth within it. First, the droplet will contact the charge collection needle. Due to the potential difference between the droplet and the bottom electrode, negative charges will be transferred to the bottom copper electrode through the copper needle, and the current flows from the external load to the bottom electrode (Fig. 2ii). Then, the droplet comes into contact with the top electrode. At this point, positive charges are transferred from the droplet to the top electrode to balance the potential difference, and the current flows from the bottom electrode to the external load (Fig. 2iii).[23] However, since the droplet is reused, charges that are not completely separated by the charge-collecting electrode will remain in the droplet. In subsequent steps, due to the presence of these free charges, during the subsequent charge separation process, a portion of opposite-sign charges will flow into the charge-collecting electrode due to the potential difference, neutralizing the previously collected charges (Fig. 2v and vii), resulting in a brief drop in the voltage signal. Immediately thereafter, normal charge separation resumes (Fig. 2vi and viii), and the voltage signal continues to rise. Eventually, as the residual charges in the droplet accumulate, charge separation becomes increasingly difficult. The output voltage reaches an equilibrium.

Based on the above working mechanism, both factors affecting the charge on the surface of triboelectric materials and factors influencing the charge on the droplets themselves can be detected using this triboelectric probe. First, the triboelectric probe is employed to monitor salt solutions of varying concentrations as well as solutions with different pH values.

It can be observed that as the pH value increases from acidic to alkaline, when the pH exceeds 4, the output electrical signal changes from a negative value to a positive one. This is
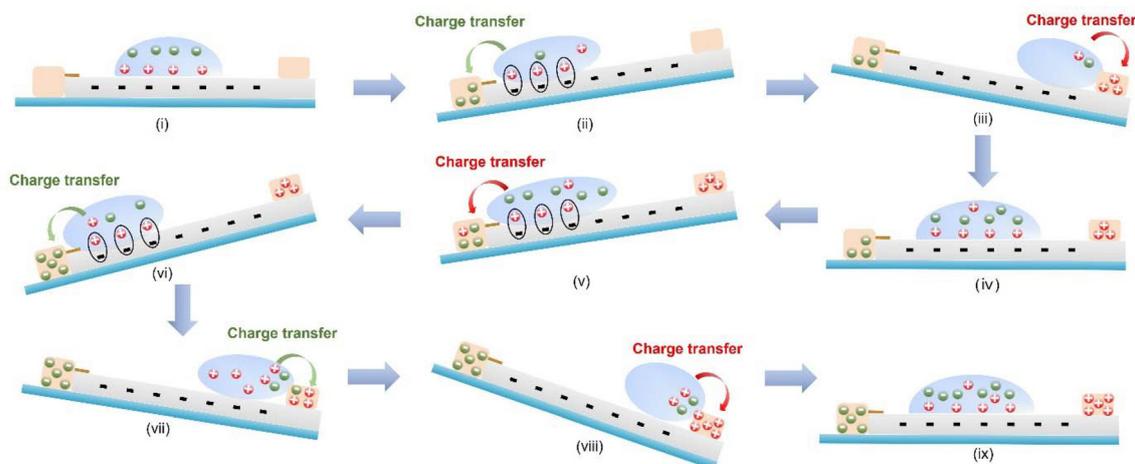

Fig. 2 Schematic diagram of the device working mechanism.

due to the isoelectric point of PDMS being around 4 (Fig. S4†); when the pH value is greater than 4, the surface of PDMS shifts from being positively charged to negatively charged. The maximum value of the output voltage when the device reaches equilibrium is achieved at a solution pH of 7 (Fig. 3a). When testing NaOH solutions, it can be observed that as the concentration increases, the output voltage at equilibrium exhibits a downward trend. Additionally, sodium chloride solutions of varying concentrations exhibit a similar trend of change (Fig. 3b). To gain a deeper understanding of the aforementioned results, it is imperative to ascertain the nature of the PDMS surface following triboelectrification under various solutions. To facilitate this, electrical double layer (EDL) models have been formulated. The isoelectric point of a substance dictates the preference for certain ions to be adsorbed onto its surface at varying pH levels. In the case of PDMS, this isoelectric point is approximately at pH 4. When the pH value is less than 4, the surface adsorbs hydrogen ions due to the excessive hydrogen ions in the solution (Fig. 3c), resulting in a positive output voltage. When the pH value is greater than 4 and below 7, the surface of PDMS shifts from being positively charged to negatively charged. When the negatively charged PDMS surface undergoes contact electrification with the solution, the amount of negative charge on the surface will be further increased, resulting in a gradual increase in voltage.

When the test solution is NaOH or NaCl, a large number of sodium ions adsorb onto the surface of the triboelectric

material due to electrostatic forces, hindering further electron transfer between the droplet and PDMS (Fig. 3c). At the same time, as the concentration of salt ions in the aqueous solution continues to increase, the conductivity of the solution becomes stronger. An increase in conductivity indicates a rise in the number of free ions within the liquid, which impairs the transfer of charge at the liquid–solid interface and, subsequently, leads to a reduction in the probe signal.[25,26] In addition, compared to NaCl solution, under the same concentration of sodium ions, NaOH solution exhibits a higher output electrical signal. This is due to the increase in the number of polar Si–O bonds on the surface of PDMS when exposed to NaOH solution, thereby enhancing triboelectric charge.[27] The aforementioned results indicate that the performance of triboelectric probes varies with the concentration of salt or alkali in the solution, demonstrating their potential for application in the field of biochemical sensors. Due to their relatively low selectivity, they are currently mainly limited to concentration sensing.

To gain a deeper understanding of the interaction between triboelectric probes and suspended particles in liquid media, we conduct tests on SiO_2 colloids at various concentrations and the results are shown in Fig. 4a. As the concentration of the SiO_2 colloid (200 nm) gradually increases, the output electrical signal exhibits a trend of first increasing and then decreasing, reaching a peak output voltage of 8.8 V at a concentration of 0.1 mg mL^{-1}. The corresponding SEM images are
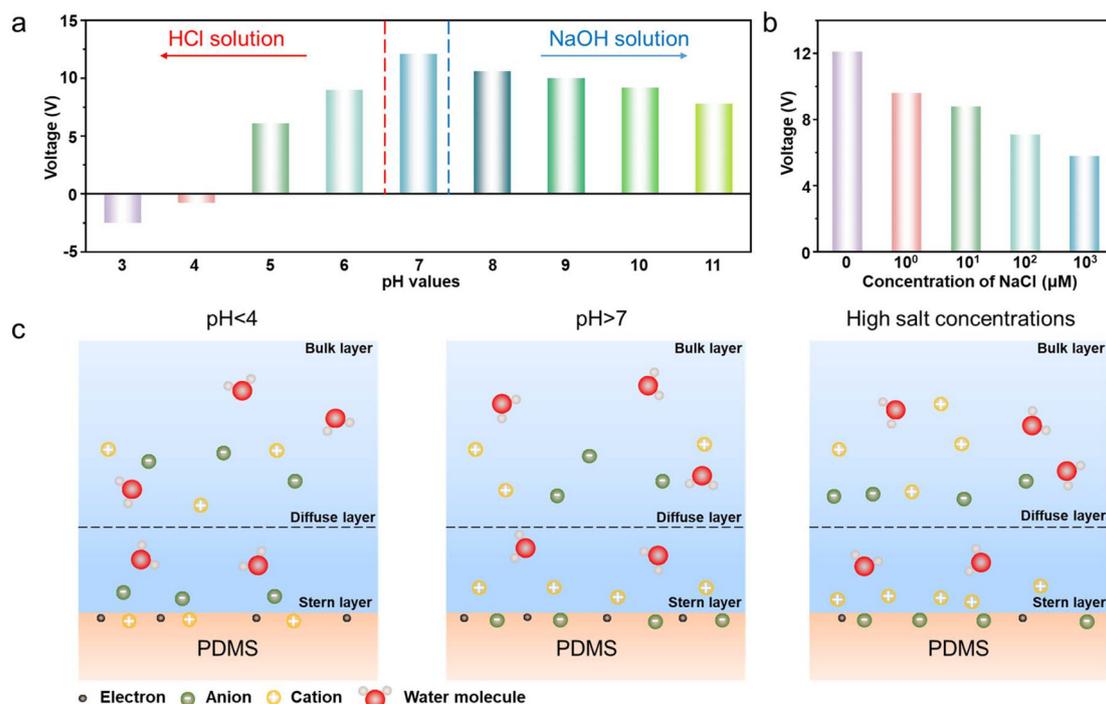

Fig. 3 Response of a self-powered device to pH and salt concentration. (a) The variation of the output voltage of a self-powered device in response to changes in the pH value of the solution (solutions with pH less than 7 are prepared with different concentrations of HCl and those with pH greater than 7 are prepared with different concentrations of NaOH.). (b) The variation of the output voltage of a self-powered sensor in response to changes in NaCl concentration. (c) Schematic diagram of the EDL structure on the PDMS surface under different conditions.
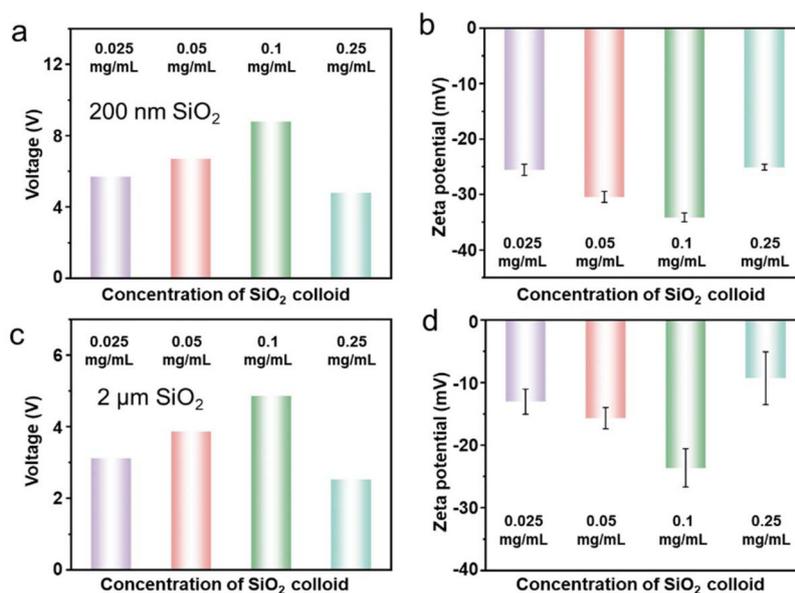
Fig. 4 Detection of SiO$_2$ colloid using the self-powered device. (a) The variation of the output voltage of the device when the solution contains SiO$_2$ colloid (with a diameter of 200 nm) of different masses. (b) Zeta potential of SiO$_2$ colloid measured at different concentrations. (c) The variation of the output voltage of the device when the solution contains SiO$_2$ colloid (with a diameter of 2 μm) of different masses. (d) Zeta potential of SiO$_2$ colloid measured at different concentrations.

displayed in Fig. S5.† The EDL of colloidal nanoparticles consists of regularly arranged and oppositely charged ions;[26] therefore, the EDL and the distribution of colloidal nanoparticles can be regarded as capacitors,[28] which will affect the macroscopic dielectric properties of the colloid.[29]

This is because the surface charge and EDL of the colloidal nanoparticles result in an increase in the relative permittivity of the SiO$_2$ colloid.[30] This process enhances the liquid's own ability to store charge. Consequently, the later time when the two processes of charge separation between the electrodes and charge storage in the droplet reach equilibrium, the higher the output voltage of the device after it stabilizes. However, as the concentration further increases, the number of free ions within the SiO$_2$ colloid increases, leading to a suppression of interfacial charge transfer between the colloid and PDMS.[30] To test this hypothesis, the zeta potentials of SiO$_2$ colloids have been measured (Fig. 4b). Compared to SiO$_2$ colloids of other concentrations, the SiO$_2$ colloid with a concentration of 0.1 mg mL^{-1} exhibits a more negative zeta potential. The reason for the above phenomenon is that at lower concentrations, as the concentration of the SiO$_2$ colloid increases, more OH– are adsorbed onto the surface of the SiO$_2$ colloid, resulting in an increase in its surface charge and a more negative zeta potential. With additional increments in the concentration of the SiO$_2$ colloid, the mutual interference between particles becomes significant, leading to the overlap of EDLs and a subsequent decrease in the surface charge and zeta potential. Furthermore, we also conducted tests on SiO$_2$ colloids with a particle size of 2 μm. The results indicated that the trends in both output voltage and zeta potential were similar to those of SiO$_2$ colloids with a particle size of 200 nm

(Fig. 4c and d). Nevertheless, in comparison with the SiO$_2$ colloid with a particle size of 200 nm, the SiO$_2$ colloid with 2 μm particles exhibited lower output voltage and zeta potential, primarily due to the more significant charge screening effect among larger particles, which subsequently led to a decrease in the zeta potential. The corresponding SEM images are displayed in Fig. S6.†

After completing tests on different concentrations of 2 μm silica colloids, it is reasonable to plan for the next step of testing *E. coli*. This is because the triboelectric probe exhibits different electrical signal responses to particles of different sizes. Furthermore, *E. coli*, as a common model organism, holds significant importance in biomedical research. Conducting triboelectric testing on different concentrations of *E. coli* can not only broaden our understanding of the response characteristics of triboelectric probes but also potentially offer new perspectives and methods for microbial detection. As shown in Fig. 5a, the output electrical signals monotonically decrease as the concentration of *E. coli* increases. When testing *E. coli* in the culture medium, the output voltage is significantly lower than that of the tap water sample at the same concentration. This is because the salt particles in the culture medium adsorb onto the surface of PDMS, impeding further charge transfer between the surface of the triboelectric material and the solution. The reason for the decreasing trend in output voltage with increasing concentration of *E. coli* in the same solution is explained as follows: on the one hand, as the concentration of *E. coli* increases, aggregation occurs among the bacteria, leading to a decrease in charge density and subsequently resulting in a reduction in zeta potential (Fig. S7†); on the other hand, *E. coli* also adheres to the
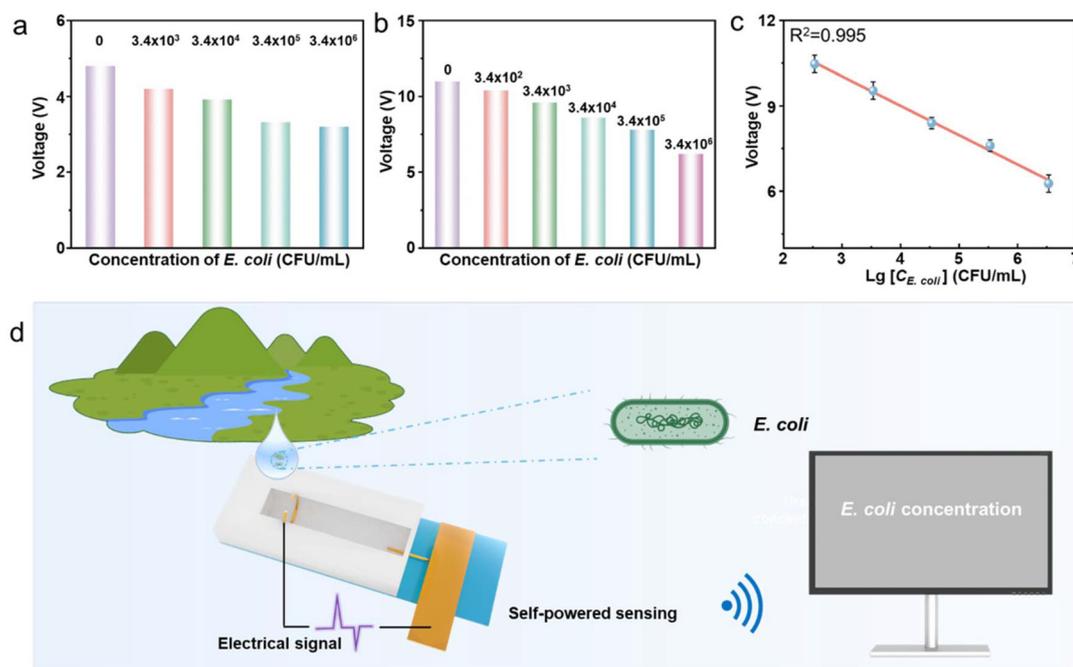
Fig. 5 The prospects of self-powered biochemical detection. (a) The variation of the output voltage of the device in response to changes in the concentration of *E. coli* in broth. (b) The variation of the output voltage of the device in response to changes in the concentration of *E. coli* in tap water. (c) The correlation of the output voltage from the self-powered sensor and *E. coli* concentrations. (d) A schematic diagram of the application of this self-powered sensor for *E. coli* concentration detection.

surface of the PDMS, both of which impede further electron transfer between the droplet and PDMS (Fig. S8†). Following the successful testing of *E. coli* samples with varying concentrations, the aim is to extend our investigation to explore the detection possibilities of *E. coli* under real environmental conditions by focusing on natural water bodies such as lake water. Specifically, lake water is intended to be used as a diluent for preparing samples containing *E. coli* at various concentrations in lake water, which will then be subjected to measurement. This operation is designed to simulate real-world detection scenarios of *E. coli* and evaluate the performance of triboelectric probes in practical applications.

As can be seen from Fig. 5b, the detection signal responses obtained for the lake water samples doped with *E. coli* exhibited similar trends. Furthermore, a good linear relationship was observed between different concentrations of *E. coli* and the output voltage (Fig. 5c), suggesting great potential for the probe in self-powered sensing of *E. coli* concentrations (Fig. 5d).

Conclusions

In this work, a solid–liquid interface based TENG with a special electrode structure was obtained by adding electrodes that can directly contact the solution at both ends of a fluid tank. Unlike conventional devices, this device utilizes the reciprocating motion of a single droplet within the device to

achieve charge accumulation in both the electrodes and the liquid sample simultaneously. Ultimately, the droplet's charge storage capacity is evaluated by the value of the output voltage when it reaches a stable state, reflecting information about the biochemical substances contained within. This device can function as a triboelectric charge-separable probe, responding to solution pH, salt concentration, and the concentration of nanoparticles or *E. coli*, demonstrating its potential as a biochemical sensor.

Experimental section

Reagents and materials

The PDMS prepolymer and curing agent were bought from Dow Corning. Conductive Cu tape with a thickness of 60 μm and Cu wire (as the charge collector needle and top electrode) with a diameter of 0.4 mm were purchased from Shenzhen Mileqi Company, China. Other chemical reagents used in this experiment were from Sinopharm Chemical Reagents Company, and the chemicals were of analytical reagent grade and utilized without further purification. Deionized water was used throughout.

Fabrication of the biosensor

The initial preparation process of the device is consistent with our previous work.[12] Then, excess PDMS is removed from the side opposite to the top electrode, and a collection needle is

inserted into the fluidic channel. Finally, copper tape is attached to one end of the collection needle.

Bacteria culturing

E. coli was dispersed in LB broth and shaken at 37 °C for 24 h. After that, the LB broth with different bacterial cells was diluted to different concentrations of 3.4×10^6, 3.4×10^5, 3.4×10^4, and 3.4×10^3 CFU mL^{-1}, for further experiments.

Characterization

The open-circuit voltage and short-circuit current were measured using a low-noise current preamplifier (SR570, Stanford Research Systems, Inc., Sunnyvale, CA, USA) and a digital phosphor oscilloscope (MSO 2024B, Tektronix, Inc., Beaverton, OR, USA). The charge transfer was measured using an electrometer (Keithley 6514, Cleveland, OH, USA). The morphologies of the as-prepared SiO_2 colloids were analyzed with a field-emission scanning electron microscope (FE-SEM) (S-4800, Hitachi, Tokyo, Japan). The zeta potential was tested using a potentiometer (Malvern).

Author contributions

Q.Z. and A.G. conceived the idea. B.W., C.P., X.Y., M.Z. and H.L. performed all experiments. Q.Z., A.G., J.P., H.Z. and F.X. discussed the outline and wrote the manuscript. All authors reviewed and approved the manuscript.

Data availability

The data that support the findings of this study are available from the corresponding author [Qitao Zhou, zhouqitao@cug.edu.cn], upon reasonable request.

Conflicts of interest

The authors declare no conflict of interest.

Acknowledgements

References

1 D. Cialla-May, X. S. Zheng, K. Weber and J. Popp, *Chem. Soc. Rev.*, 2017, **46**, 3945–3961.

2 S. Mittal, H. Kaur, N. Gautam and A. K. Mantha, *Biosens. Bioelectron.*, 2017, **88**, 217–231.

3 J.-C. Dong, X.-G. Zhang, V. Briega-Martos, X. Jin, J. Yang, S. Chen, Z.-L. Yang, D.-Y. Wu, J. M. Feliu and C. T. Williams, *Nat. Energy*, 2019, **4**, 60–67.

4 C. J. Chang, T. D. James, E. J. New and B. Z. Tang, *Acc. Chem. Res.*, 2020, **53**, 1.

5 Y. F. Huang, P. J. Kooyman and M. T. Koper, *Nat. Commun.*, 2016, **7**, 1–7.

6 T. Rasheed and F. Nabeel, *Coord. Chem. Rev.*, 2019, **401**, 213065.

7 F. Xie, M. Yang, M. Jiang, X.-J. Huang, W.-Q. Liu and P.-H. Xie, *Trends Anal. Chem.*, 2019, **119**, 115624.

8 J. Pan, W. Xu, Y. Zhang, Y. Ke, J. Dong, W. Li, L. Wang, B. Wang, B. Meng, Q. Zhou and F. Xia, *Nano Energy*, 2024, **132**, 110412.

9 R. Liu, Z. L. Wang, K. Fukuda and T. Someya, *Nat. Rev. Mater.*, 2022, **7**, 870–886.

10 J. Min, S. Demchyshyn, J. R. Sempionatto, Y. Song, B. Hailegnaw, C. Xu, Y. Yang, S. Solomon, C. Putz, L. E. Lehner, J. F. Schwarz, C. Schwarzinger, M. C. Scharber, E. Shirzaei Sani, M. Kaltenbrunner and W. Gao, *Nat. Electron.*, 2023, **6**, 630–641.

11 X.-S. Zhang, M. Han, B. Kim, J.-F. Bao, J. Brugger and H. Zhang, *Nano Energy*, 2018, **47**, 410–426.

12 M. Wang, J. Zhang, Y. Tang, J. Li, B. Zhang, E. Liang, Y. Mao and X. Wang, *ACS Nano*, 2018, **12**, 6156–6162.

13 B. Zhang, Y. Jiang, T. Ren, B. Chen, R. Zhang and Y. Mao, *Int. J. Extreme Manuf.*, 2024, **6**, 062003.

14 C. Ning, L. Tian, X. Zhao, S. Xiang, Y. Tang, E. Liang and Y. Mao, *J. Mater. Chem. A*, 2018, **6**, 19143–19150.

15 M. Wang, N. Zhang, Y. Tang, H. Zhang, C. Ning, L. Tian, W. Li, J. Zhang, Y. Mao and E. Liang, *J. Mater. Chem. A*, 2017, **5**, 12252–12257.

16 A. Gao, Q. Zhou, Z. Cao, W. Xu, K. Zhou, B. Wang, J. Pan, C. Pan and F. Xia, *Adv. Sci.*, 2024, **11**, 2309824.

17 Q. Zhou, B. Wang, A. Gao, W. Xu, K. Zhou, J. Pan, G. Meng, C. Pan and F. Xia, *Adv. Funct. Mater.*, 2022, **32**, 2209100.

18 S. Lin, L. Xu, A. Wang and Z. L. Wang, *Nat. Commun.*, 2020, **11**, 399.

19 W. Xu, H. Zheng, Y. Liu, X. Zhou, C. Zhang, Y. Song, X. Deng, M. Leung, Z. Yang, R. X. Xu, Z. L. Wang, X. C. Zeng and Z. Wang, *Nature*, 2020, **578**, 392.

20 X. Xu, Y. Wang, P. Li, W. Xu, L. Wei, Z. Wang and Z. Yang, *Nano Energy*, 2021, **90**, 106573.

21 J. Dong, L. Zhu, P. Guo, C. Xu, X. Zhao, S. Yang, X. He, G. Zhou, G. Ma, H. Guo, C. Hu and Q. Song, *Energy Environ. Sci.*, 2023, **16**, 1071–1081.

22 J. Dong, C. Xu, L. Zhu, X. Zhao, H. Zhou, H. Liu, G. Xu, G. Wang, G. Zhou, Q. Zeng and Q. Song, *Nano Energy*, 2021, **90**, 106567.

23 T. Liu, W. Mo, X. Zou, B. Luo, S. Zhang, Y. Liu, C. Cai, M. Chi, J. Wang, S. Wang, D. Lu and S. Nie, *Adv. Funct. Mater.*, 2023, **33**, 2304321.

24 S. Lin, X. Chen and Z. L. Wang, *Chem. Rev.*, 2022, **122**, 5209–5232.

25 B. Luo, T. Liu, C. Cai, J. Yuan, Y. Liu, C. Gao, X. Meng, J. Wang, S. Zhang, M. Chi, Y. Qin, J. Zhao, X. Zhuang, S. Wang and S. Nie, *Nano Energy*, 2023, **113**, 108532.

26 L. Zhang, X. Li, Y. Zhang, Y. Feng, F. Zhou and D. Wang, *Nano Energy*, 2020, **78**, 105370.

27 B. K. Yun, J. W. Kim, H. S. Kim, K. W. Jung, Y. Yi, M.-S. Jeong, J.-H. Ko and J. H. Jung, *Nano Energy*, 2015, **15**, 523–529.

28 M. D. Parvez Ahmad, A. Venkateswara Rao, K. Suresh Babu and G. Narsinga Rao, *Mater. Chem. Phys.*, 2019, **224**, 79–84.

29 H. Luo, H. Wang, L. Yang, H. Wu, S. Kang, S. Yong, R. Liao, J. Wang and Z. L. Wang, *Adv. Funct. Mater.*, 2022, **32**, 2200862.

30 B. Luo, C. Cai, T. Liu, S. Zhang, C. Gao, Y. Liu, M. Chi, J. Wang, S. Wang and S. Nie, *Nano Energy*, 2023, **117**, 108874.